Exploiting a robust biopolymer network binder for an ultrahigh-areal-capacity Li–S battery†

Jie Liu,[a] Dilini G. D. Galpaya,[b] Lijing Yan,[a] Minghao Sun,[a] Zhan Lin,[*a] Cheng Yan,[b] Chengdu Liang[a] and Shanqing Zhang[*c]

High-loading electrodes play a crucial role in the practical applications of high-energy-density batteries,which are especially challenging for lithium–sulfur (Li–S) batteries. Herein, a mechanically robust network binder was constructed by weaving dual biopolymers (i.e., guar gum and xanthan gum) via the intermolecular binding effect of extensive functional groups in both polymers. This network binder was capable of effectively preventing polysulfides within the electrode from shuttling and, consequently, improved electrochemical performance. A remarkably high sulfur loading of 19.8 mg cm^{-2} and an ultrahigh areal capacity of 26.4 mA h cm^{-2} were achieved as a result of the robust mechanical properties of the network binder. This study paves a new way for obtaining high-energy-density batteries by the simple application of robust network biopolymer binders that are inherently low-cost and environmentally friendly.

Broader context

High-energy-density energy storage devices are imperative in the rapid development of electric vehicles, hybrid electric vehicles, and smart power grids. Li–S batteries with a high theoretical capacity of 1675 mA h g^{-1} are promising candidates. To achieve high-energy-density Li–S batteries, high-loading sulphur electrodes are required. However, problems with Li–S batteries, including the shuttle effect, a huge volume change during charge and discharge processes, and the insulating property of sulfur, become more serious in high-loading Li–S batteries. Moreover, thick electrode films tend to fracture and delaminate from the current collector during the cycling process. In contrast to previously reported approaches, we propose a new, facile, and effective approach to obtaining high loading Li–S batteries by exploiting a robust biopolymer network binder. Furthermore, the biopolymer network binder has the advantages of being low-cost, environmentally friendly, and water-soluble. The concept in this study can simultaneously address energy and environmental issues, and the biopolymer network binder is promising for the future development of high-energy-density batteries.

---

[a] Key Laboratory of Biomass Chemical Engineering of Ministry of Education, College of Chemical and Biological Engineering, Zhejiang University,Hangzhou 310027, China.
E-mail: hanlin@zju.edu.cn
[b] School of Chemistry, Queensland University of Technology, QLD 4001, Australia
[c] Centre for Clean Environment and Energy, Environmental Futures Research Institute and Griffith School of Environment, Gold Coast Campus,Griffith University, QLD 4222, Australia.
E-mail: s.zhang@griffith.edu.au

The ever-increasing demand for portable electronic devices, electric vehicles, and hybrid electric vehicles is triggering the development of advanced energy storage devices with high energy densities.[1,2] Generally, areal capacity determines the total capacity per electrode and consequently the energy density of a battery.[3] Therefore, the increasing demand for high energy densities has driven the battery community to exploit highareal-capacity electrodes. Sulfur cathodes, which have a high theoretical capacity of 1675 mA h g^{-1}, lead to a high theoretical specific energy of 2567 W h kg^{-1} when combined with metallic lithium anodes, and this combination is considered a highly promising candidate.[4,5]

Developing high-loading electrodes is an effective way to increase areal capacity and, therefore, the energy density of batteries. However, as the amount of areal loading increases, the electrode film on the current collector becomes thicker. The thick electrode tends to fracture and delaminate from the current collector after coating and drying, making the high-loading electrode more difficult to realize.[6,7] Moreover, the issues of lithium–sulfur (Li–S) batteries, including the formation of soluble long-chain polysulfides that easily diffuse out of the cathode scaffold and cause shuttle reactions, the insulator nature of the sulfur material, and the huge volume change (76%) during charge and discharge,[8–10] become more serious in high-loading Li–S batteries. Only through applying a well-designed electrode structure can high-loading Li–S batteries be obtained. Three-dimensional (3D) porous current collectors,[7,11] layer-by-layer structured electrodes,[12,13] and functional separators[14] have been exploited to realize high-loading Li–S batteries. Among them, a highest areal capacity of 23.3mA h cm^{-2} was obtained with a sulfur loading of 21.2 mg cm^{-2}; however, the well-designed electrode structures used complicated preparation process and were not suitable for widespread applications.

As an electrode component, binders play a crucial role in improving electrochemical performance. Normally, binders bond active materials and conductive additives together on current collectors and keep electrode films integrated to ensure repeatable operation of the battery. More specifically, binder functional groups interact with active material to enhance electrochemical performance. Owing to hydrogen bonding between the binder functional groups and SiO_x layers on the Si active material surface, the cycling stability of Si anodes in Li-ion battery is markedly enhanced.[15–18] Various polymers, such as gelatin,[19] poly(ethylene oxide),[20] and carbonyl-b-cyclodextrin,[21] have been applied as binders in Li–S batteries to replace conventional polyvinylidene fluoride (PVDF) binder and improve electrochemical performance. A binder with oxygenous functional groups effectively constrains polysulfides, prevents the shuttle effect, and dramatically improves cycling stability in the Li–S battery.[22] Therefore, we propose that a high-energy-density battery with a high-loading active material can be achieved by exploiting an effective binder.

Herein, in order to confirm our concept, we intentionally prepared a 3D network binder (denoted as N-GG-XG binder) using the intermolecular binding effect between guar gum (GG) and xanthan gum (XG) for high-loading Li–S batteries. GG is a polysaccharide derived from the endosperm of seeds of *Cyamopsis tetragonolobus*, and XG is an extracellular polysaccharide excreted by the bacterium *Xanthomonas campestris*.[23,24] Both biopolymers are non-toxic, low-cost, sustainable natural products. Both GG and XG contain large amounts of oxygen-containing functional groups, as shown in Fig. 1a and b, which can effectively bind polysulfides. Owing to the intermolecular binding effect between GG and XG, a robust biopolymer network is formed,[25,26] providing the strong mechanical capability to support up to 19.8 mg cm^{-2} of sulfur active material and, therefore, realize an ultrahigh areal specific capacity of 26.4 mA h cm^{-2}. To our knowledge, this is the first time that such a high-loading Li–S battery has been achieved by simply applying a polymer binder. Furthermore, the N-GG-XG binder facilitated electrode fabrication in a water-based environmentally friendly process. Therefore, this new concept addresses environmental and energy issues simultaneously, and could provide a new way to access high-energy-density batteries of high-loading active materials.

The binder functional groups are important when binding polysulfides and improving the cycling performance of Li–S batteries.[22] Therefore, GG and XG, which both contain large amounts of oxygen-containing functional groups, were chosen for this study. The chemical structures of GG and XG are displayed in Fig. 1a and b, respectively. GG consists of linear chains of (1-4)-β-D-mannopyranosyl units with α-D-galactopyranosyl units attached through (1→6) linkages.[23,27] XG is composed of D-glucosyl, D-mannosyl, and D-glucuronyl acid residues in a molar ratio of 2 : 2 : 1 and variable amounts of *O*-acetyl and pyruvyl residues.[28,29] In aqueous solution, the hydrophobicity of the XG main backbone, along with a series of inter/intramolecular hydrogen bonding interactions, leads to double helix formation.18,30 Normally, galactose residues are not uniformly distributed in GG molecules. Some regions contain many galactose residues (hairy regions) and others have no galactose residues (smooth regions). In the smooth regions, copolymer interactions between GG and XG can take place,[25,26,31] as illustrated in Fig. 1c. Consequently, a mechanically robust biopolymer network is formed (Fig. 1d) to support a high-loading sulfur active material.

The intermolecular binding effect between GG and XG was studied by Fourier transform infrared (FTIR) spectroscopy. The peak assigned to a specific functional group in the FTIR spectrum shifts to either a higher or lower wavenumber, or a new peak (or shoulder) appears, when an interaction takes place in the material. Fig. 1e compares the FTIR spectra of GG, XG, and N-GG-XG. GG shows a broad absorption band at 3431 cm^{-1}, ascribed to O–H stretching, a peak at 1152 cm^{-1}, corresponding to a C–OH stretching mode, and a peak at 1074 cm^{-1}, corresponding to CH_2–OH stretching.[32,33] XG shows a broad absorption band at 3433 cm^{-1}, due to O–H stretching. The absorption bands at 1726 cm^{-1} and 1621 cm^{-1} were attributed to the stretching of the carbonyl (C=O) ester in the acetyl group and asymmetric CQO stretching in the carboxylate group, respectively.[34] Compared with GG, in N-GG-XG, the O–H stretching band shifted to a higher wavenumber (3444 cm^{-1}), and the absorption bands attributed to carbonyl stretching in the acetyl ester group and carboxylate group appeared and shifted to 1718 cm^{-1} and 1630 cm^{-1}, respectively, indicating that interactions between GG and XG had occurred.[35] Changes in peak intensities in the XRD patterns (Fig. S1, ESI†) further demonstrated the rearrangement of biopolymer molecule chains due to network formation by GG and XG.[36] In Fig. S2 (ESI†), water-soluble N-GG-XG displayed an observably higher viscosity than the viscosity calculated from the mass ratio of GG and XG in N-GG-XG (3:1), also indicating the intermolecular binding effect between GG and XG.

Electrochemical tests were carried out to evaluate the application of N-GG-XG as a binder in Li–S batteries. The electrochemical stability of N-GG-XG was first studied using cyclic voltammetry (CV), as shown in Fig. S3 (ESI†), which demonstrated that the N-GG-XG binder was inactive between 1.5 and 2.8 V. Fig. 2a displays charge–discharge curves of the S@N-GG-XG electrode with a sulfur loading of 0.78 mg cm^{-2} at 0.5C, which is a common sulfur loading in the study of Li–S batteries.[9,10,22] This sulfur electrode gave the two-plateau discharge curve typical of conventional Li–S cells, i.e., the formation of soluble long-chain polysulfides (Li_2S_x, $4 \leq x \leq 8$) at about 2.3 V and insoluble short-chain Li2S2/Li2S at around 2.1 V,[8,9] which agreed well with the CV curves of the S@N-GG-XG electrode (Fig. 2b). Therefore, the N-GG-XG polymer could be used as a binder for Li–S batteries.

GG and XG have been reported as high-performance binders for Si anodes in Li-ion batteries, [16, 18] making them potential binders for Li–S batteries, due to their extensive functional groups. Fig. 2c indicates that the S@GG and S@XG electrodes show good cycling performances; however, both were inferior to the S@N-GG-XG electrode. Compared with commonly used binders (e.g., gelatin and PVDF) in sulfur electrodes, the S@N-GG-XG electrode showed greatly improved cycling stability, with a discharge capacity of 913 mA h g^{-1} after 60 cycles at 0.5C, which was 452 mA h g^{-1} higher than that of the S@gelatin electrode and 277 mA h g^{-1} higher than that of the S@PVDF electrode. In a prolonged cycling test, the

S@N-GG-XG electrode still delivered a capacity of 724 mA h g^{-1} after 150 cycles (Fig. 2e). Moreover, the S@N-GG-XG electrode showed an outstanding rate capability, with a capacity of 737 mA h g^{-1} at 5C, as displayed in Fig. 2d. The improved cycling performance of the S@N-GG-XG electrode was mainly due to the network structure of the N-GG-XG binder. In contrast to linear polymer binders, large numbers of oxygen containing functional groups in the N-GG-XG binder formed a network of interaction sites to bind polysulfides more effectively.

Generally, areal capacity determines the total capacity of an electrode and, consequently, the energy density of a battery. Therefore, a high-loading sulfur electrode was prepared via a common doctor blade coating method on a Ni foam current collector, which worked as the scaffold to avert electrode crimping in the case of a thick electrode film. However, the hydrophobicity of Ni foam restricts the permeation of slurry into the interior of the current collector. As a consequence, a thick and pyknotic electrode film was formed on the surface of the Ni foam current collector (Fig. S4, ESI†). The high-loading sulfur electrodes also display typical charge–discharge curves of conventional Li–S batteries, as shown in Fig. S5 (ESI†). The S@N-GG-XG electrode with a sulfur loading of 6.5 mg cm^{-2} showed superior cycling stability and delivered a discharge capacity of 652 mA h g^{-1} after 90 cycles at 0.8 mA cm^{-2}, corresponding to an areal capacity of 4.2 mA h cm^{-2} (Fig. 3a and b). In contrast, the S@GG, S@XG, S@gelatin, and S@PVDF electrodes showed rapid capacity fading after fewer cycles (S@GG electrode, 50 cycles; S@XG electrode, 25 cycles; S@gelatin electrode, 25 cycles; and S@PVDF electrode, 15 cycles). Furthermore, with a higher sulfur loading of 11.9 mg cm^{-2}, the S@N-GG-XG electrode still showed stable cycling performance, with a discharge capacity of 733 mA h g^{-1} after 60 cycles at 1.6 mA cm^{-2}, corresponding to an areal capacity of 8.7 mA h cm^{-2} (Fig. 3c). Meanwhile, the S@N-GG-XG electrode showed a high coulombic efficiency of about 94% after 60 cycles (Fig. 3d). It is worth noting that, in this study, a common super P carbon, whose deficiency of pore structure and low surface area led to a low sulfur adsorption capacity, was used as conductive matrix. Furthermore, only a small amount of $LiNO_3$ (1.5 wt%), known to effectively suppress the shuttle effect,[37] was added to the electrolyte to investigate the effect of the binder on electrochemical performance.

The disparity in electrochemical performance was mainly due to the different binder characteristics. An evaluation of the mechanical properties was carried out using nanoscratch and nanoindentation tests with scanning probe microscopy (SPM). The in situ 3D images of nanoscratch impressions of sulphur electrodes with different binders are shown in Fig. 4a and Fig. S6 (ESI†). The images of the sulfur electrodes with different binders after scratch tests showed drastic differences. The scratch track of the S@N-GG-XG electrode was smooth, with limited cracks in the laminate. In contrast, the other electrodes showed irregular distribution patterns in their scratch tracks. Because the scratch test simulates stress induced by volume changes, this result demonstrated that the N-GG-XG binder was more tolerant to volume changes than other binders. Moreover, the high friction coefficients of the S@N-GG-XG electrode implied the high adhesive force of the N-GG-XG binder (Fig. 4b). The nanoindentation test was carried out under a force of 500 mN and 10 individual indents were adopted for accurate calculation of the reduced modulus and hardness. The average reduced modulus and hardness for sulfur electrodes with different binders are shown in Fig. 4c and d, respectively. The S@N-GG-XG electrode showed higher reduced modulus and hardness, which favoured the improved cycling performance of active materials with huge volume changes.[15,16] However, an excessively high reduced modulus of S@gelatin electrode might make it brittle and cause poor cycling performance. Fig. S7–S9 (ESI†) display the different characteristics of binders and that the mechanically robust N-GG-XG binder effectively integrates the high-loading sulfur electrode, which ensures repeatable battery operation. The insignificant swelling property in the electrolyte of the rigid N-GG-XG binder also contributed to the excellent stability of the electrode structure during charge and discharge processes (Fig.

S10, ESI†).[38] In scenarios with high sulfur loading and low binder content (10 wt%) in the electrode, the shuttle effect still occurred, leading to a rough Li anode (Fig. S11, ESI†). To further confirm the concept proposed in this study, we increased the loading of sulfur active material to 19.8 mg cm^{-2}. Batteries with these S@N-GG-XG electrodes still charged and discharged normally, and delivered an ultrahigh initial areal capacity of 26.4 mA h cm^{-2}, as shown in Fig. 5a. We believe that cycling performance could be further improved by combination with a porous carbon conductive matrix and more $LiNO_3$ additive. Such a high sulfur loading is unprecedented in previous studies of binders for Li–S batteries, as displayed in Fig. 5b and Table S1 (ESI†). In comparison with studies applying well-designed electrode structures to obtain high-loading sulfur cathodes, our work still achieves very high sulfur loading and ultrahigh areal specific capacity (Fig. 5c). As a proof of concept, the charge storage capability of the as-prepared high-loading Li–S battery was demonstrated by powering an electronic stopwatch (Fig. 5d). The inset in Fig. 5d shows that the high-loading Li–S battery powered a light emitting diode, indicating a high operating voltage. This high energy density achieved by the high-loading Li–S battery demonstrated the practical application potential of this robust N-GG-XG binder in high-loading electrodes.

In conclusion, high-loading sulfur electrodes with high energy densities were readily prepared through the application of a robust N-GG-XG binder, which was synthesized using the intermolecular binding effect between GG and XG. This N-GG-XG binder was low-cost and environmentally friendly, and contained a large number of oxygen-containing functional groups to improve cycling performance. The robust mechanical properties of the N-GG-XG binder resulted in a high-sulfur-loading electrode of 19.8 mg cm^{-2} with an ultrahigh areal specific capacity of 26.4 mA h cm^{-2}. These results confirmed our concept that a highenergy-density battery can be simply obtained using a facile and effective binder. This work will inspire the battery community to explore novel binders for high-energy-density batteries.

Acknowledgements

Z. Lin thanks the Chinese government for funding support under the ‘‘Thousand Youth Talents Program’’, the Zhejiang Province Science Fund for Distinguished Young Scholars (Project LR16B060001), and the Key Technology and Supporting Platform for Genetic Engineering of Materials under the State’s Key Project of Research and Development Plan (Project 2016YFB0700600).

References

1 L. Xiao, Y. Cao, J. Xiao, B. Schwenzer, M. H. Engelhard, L. V. Saraf, Z. Nie, G. J. Exarhos and J. Liu, Adv. Mater., 2012, 24, 1176–1181.
2 W. Zhou, Y. Yu, H. Chen, F. J. DiSalvo and H. D. Abrun˜a, J. Am. Chem. Soc., 2013, 135, 16736–16743.
3 R. Yi, J. Zai, F. Dai, M. L. Gordin and D. Wang, Nano Energy, 2014, 6, 211–218.
4 S. Evers and L. F. Nazar, Acc. Chem. Res., 2013, 46, 1135–1143.
5 X. Wang, G. Li, J. Li, Y. Zhang, A. Wook, A. Yu and Z. Chen, Energy Environ. Sci., 2016, 9, 2533–2538.
6 L. Qie, C. Zu and A. Manthiram, Adv. Energy Mater., 2016, 6, 1502459.
7 G. Zhou, L. Li, C. Ma, S. Wang, Y. Shi, N. Koratkar, W. Ren, F. Li and H. M. Cheng, Nano Energy, 2015, 11, 356–365.
8 G. Xu, B. Ding, L. Shen, P. Nie, J. Han and X. Zhang, J. Mater. Chem. A, 2013, 1, 4490–4496.

9 N. Li, M. Zheng, H. Lu, Z. Hu, C. Shen, X. Chang, G. Ji, J. Cao and Y. Shi, Chem. Commun., 2012, 48, 4106–4108.
10 J. Q. Huang, Q. Zhang, H. J. Peng, X. Y. Liu, W. Z. Qian and F. Wei, Energy Environ. Sci., 2014, 7, 347–353.
11 X. B. Cheng, H. J. Peng, J. Q. Huang, L. Zhu, S. H. Yang, Y. Liu, H. W. Zhang, W. Zhu, F. Wei and Q. Zhang, J. Power Sources, 2014, 261, 264–270.
12 L. Qie and A. Manthiram, Adv. Mater., 2015, 27, 1694–1700.
13 Z. Yuan, H. J. Peng, J. Q. Huang, X. Y. Liu, D. W. Wang, X. B. Cheng and Q. Zhang, Adv. Funct. Mater., 2014, 24, 6105–6112.
14 C. H. Chang, S. H. Chung and A. Manthiram, Small, 2016, 12, 174–179.
15 I. Kovalenko, B. Zdyrko, A. Magasinski, B. Hertzberg, Z. Milicev, R. Burtovyy, I. Luzinov and G. Yushin, Science, 2011, 334, 75–79.
16 J. Liu, Q. Zhang, T. Zhang, J. T. Li, L. Huang and S. G. Sun, Adv. Funct. Mater., 2015, 25, 3599–3605.
17 M. H. Ryou, J. Kim, I. Lee, S. Kim, Y. K. Jeong, S. Hong, J. H. Ryu, T. S. Kim, J. K. Park, H. Lee and J. W. Choi, Adv. Mater., 2013, 25, 1571–1576.
18 Y. K. Jeong, T. W. Kwon, I. Lee, T. S. Kim, A. Coskun and J. W. Choi, Energy Environ. Sci., 2015, 8, 1224–1230.
19 J. Sun, Y. Huang, W. Wang, Z. Yu, A. Wang and K. Yuan, Electrochim. Acta, 2008, 53, 7084–7088.
20 S. E. Cheon, J. H. Cho, K. S. Ko, C. W. Kwon, D. R. Chang, H. T. Kim and S. W. Kim, J. Electrochem. Soc., 2002, 149, A1437–A1441.
21 J. Wang, Z. Yao, C. W. Monroe, J. Yang and Y. Nuli, Adv. Funct. Mater., 2013, 23, 1194–1201.
22 G. Li, M. Ling, Y. Ye, Z. Li, J. Guo, Y. Yao, J. Zhu, Z. Lin and S. Zhang, Adv. Energy Mater., 2015, 5, 1500878.
23 Y. S. R. Krishnaiah, V. Satyanarayana, B. D. Kumar and R. S. Karthikeyan, Eur. J. Pharm. Sci., 2002, 16, 185–192.
24 A. B. Rodd, D. E. Dunstan and D. V. Boger, Carbohydr. Polym., 2000, 42, 159–174.
25 D. Xue and R. Sethi, J. Nanopart. Res., 2012, 14, 1239.
26 F. G. Ochoa, V. E. Santos, J. A. Casas and E. Go´mez, Biotechnol. Adv., 2000, 18, 549–579.
27 B. Heyman, W. H. D. Vos, F. Depypere, P. V. D. Meeren and K. Dewettinck, Food Hydrocolloids, 2014, 35, 546–556.
28 S. Rosalam and R. England, Enzyme Microb. Technol., 2006, 39, 197–207.
29 V. B. Bueno, R. Bentini, L. H. Catalani and D. F. S. Petri, Carbohydr. Polym., 2013, 92, 1091–1099.
30 N. M. Sereno, S. E. Hill and J. R. Mitchell, Carbohydr. Res., 2007, 342, 1333–1342.
31 D. Kim, M. Quinlan and T. F. Yen, Waste Manage. 2009, 29, 321–328.
32 D. Mudgil, S. Barak and B. S. Khatkar, Int. J. Biol. Macromol., 2012, 50, 1035–1039.
33 M. Velimirovic, H. Chen, Q. Simons and L. Bastiaens, J. Contam. Hydrol., 2012, 142–143, 1–10.
34 A. M. S. Maia, H. V. M. Silva, P. S. Curti and R. C. Balaban, Carbohydr. Polym., 2012, 90, 778–783.
35 B. Koo, H. Kim, Y. Cho, K. T. Lee, N. S. Choi and J. Cho, Angew. Chem., Int. Ed., 2012, 51, 8762–8767.
36 J. Liu, Q. Zhang, Z. Y. Wu, J. H. Wu, J. T. Li, L. Huang and S. G. Sun, Chem. Commun., 2014, 50, 6386–6389.
37 S. S. Zhang, Electrochim. Acta, 2012, 70, 344–348.
38 S. S. Zhang, J. Electrochem. Soc., 2012, 159, A1226–A1229.

39 M. J. Lacey, F. Jeschull, K. Edstro¨m and D. Brandell, J. Power Sources, 2014, 264, 8–14.
40 G. Ai, Y. Dai, Y. Ye, W. Mao, Z. Wang, H. Zhao, Y. Chen, J. Zhu, Y. Fu, V. Battaglia, J. Guo, V. Srinivasan and G. Liu, Nano Energy, 2015, 16, 28–37.
41 P. Bhattacharya, M. I. Nandasiri, D. Lv, A. M. Schwarz, J. T. Darsell, W. A. Henderson, D. A. Tomalia, J. Liu, J. G. Zhang and J. Xiao, Nano Energy, 2016, 19, 176–186.
42 X. Duan, Y. Han, Y. Li and Y. Chen, RSC Adv., 2014, 4, 60995–61000.
43 J. Pan, G. Xu, B. Ding, J. Han, H. Dou and X. Zhang, RSC Adv., 2015, 5, 13709–13714.
44 J. Pan, G. Xu, B. Ding, Z. Chang, A. Wang, H. Dou and X. Zhang, RSC Adv., 2016, 6, 40650–40655.
45 Z. Li, J. T. Zhang, Y. M. Chen, J. Li and X. W. Lou, Nat. Commun., 2015, 6, 8850.
46 G. Zhou, E. Paek, G. S. Hwang and A. Manthiram, Nat. Commun., 2015, 6, 7760.
47 N. Osada, C. B. Bucur, H. Aso and J. Muldoon, Energy Environ. Sci., 2016, 9, 1668–1673.
48 R. Fang, S. Zhao, P. Hou, M. Cheng, S. Wang, H. M. Cheng, C. Liu and F. Li, Adv. Mater., 2016, 28, 3374–3382.
49 G. Hu, C. Xu, Z. Sun, S. Wang, H. M. Cheng, F. Li and W. Ren, Adv. Mater., 2016, 28, 1603–1609.
50 S. S. Zhang, Electrochem. Commun., 2013, 31, 10–12.
51 R. Fang, S. Zhao, S. Pei, X. Qian, P. X. Hou, H. M. Cheng, C. Liu and F. Li, ACS Nano, 2016, 10, 8676–8682.
52 H. J. Peng, W. T. Xu, L. Zhu, D. W. Wang, J. Q. Huang, X. B. Cheng, Z. Yuan, F. Wei and Q. Zhang, Adv. Funct. Mater., 2016, 26, 6351–6358.
53 H. J. Peng, D. W. Wang, J. Q. Huang, X. B. Cheng, Z. Yuan, F. Wei and Q. Zhang, Adv. Sci., 2016, 3, 1500268.
54 S. H. Chung, C. H. Chang and A. Manthiram, Energy Environ. Sci., 2016, 9, 3188–3200.

Figures

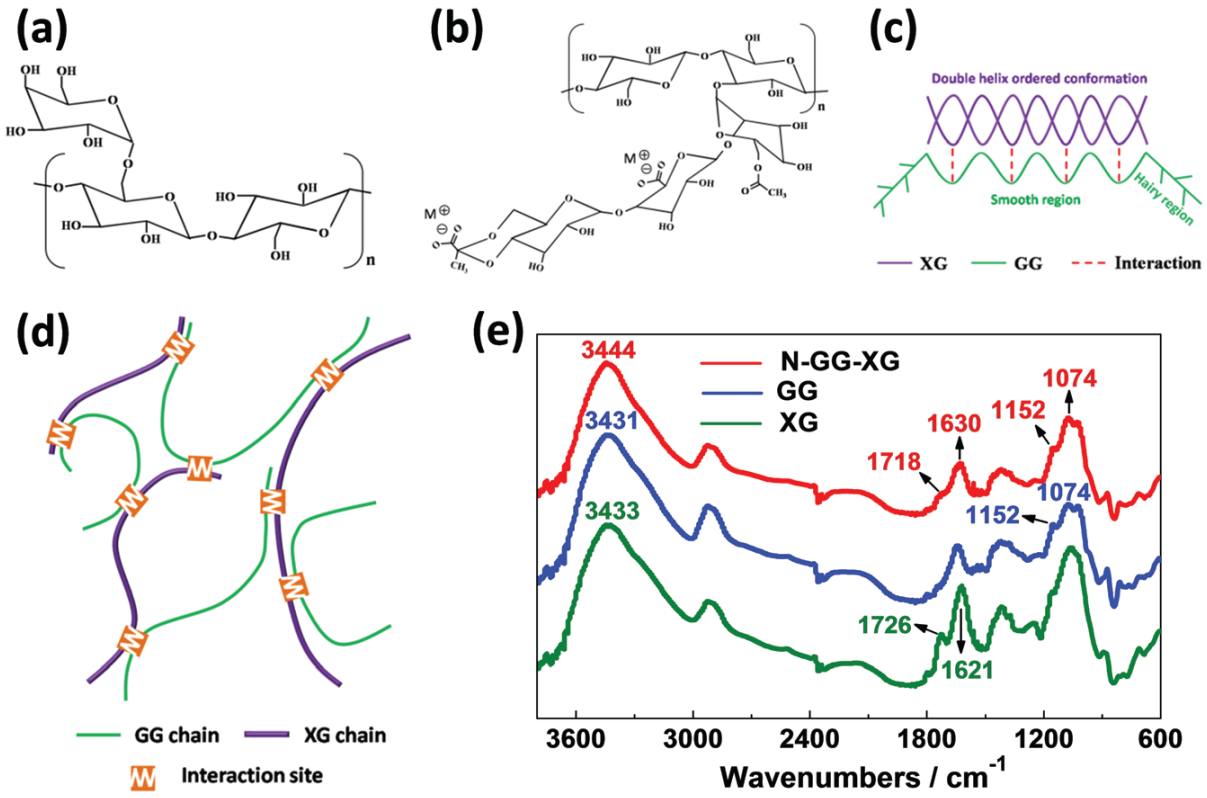

Fig. 1 Chemical structures of (a) GG and (b) XG; (c) schematic of the intermolecular binding effect between GG and XG; (d) schematic of the polymer network formed by the intermolecular binding effect; and (e) FTIR spectra of GG, XG, and N-GG-XG.

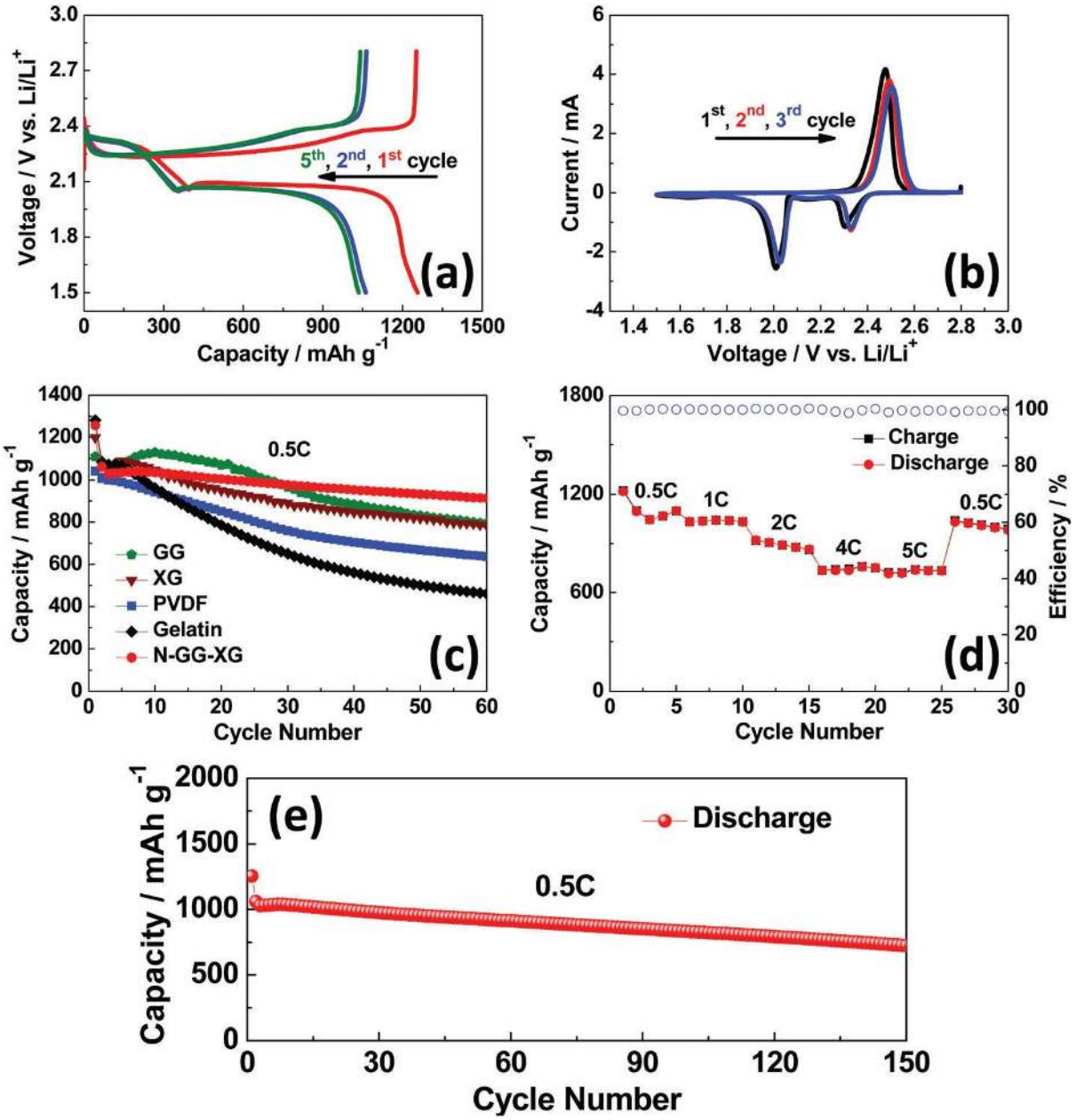

Fig. 2 (a) Charge–discharge curves of the S@N-GG-XG electrode at 0.5C; (b) CV curves of the S@N-GG-XG electrode at a scan rate of 0.1 mV s^{-1}; (c) cycling performance of sulfur cathodes with different binders at 0.5C; (d) rate performance of the S@N-GG-XG electrode; (e) prolonged cycling performance of the S@N-GG-XG electrode at 0.5C.

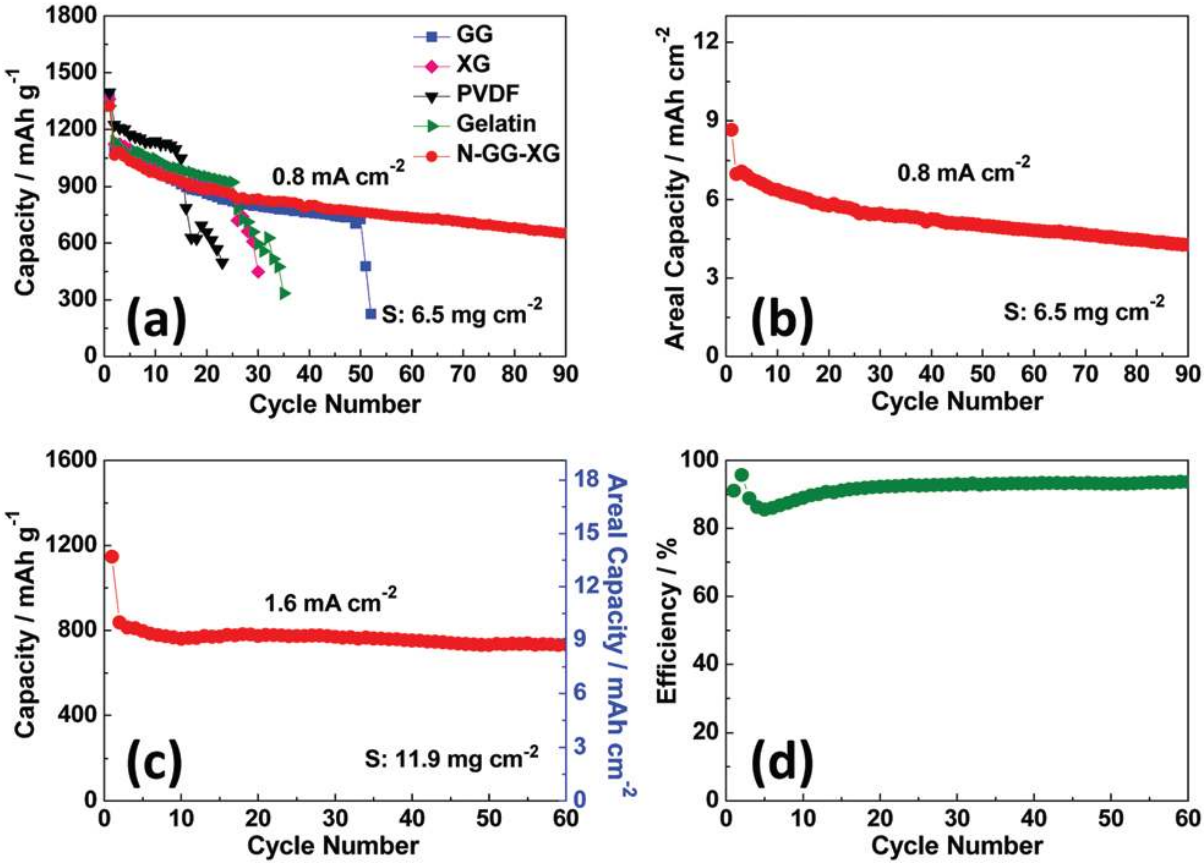

Fig. 3 (a) Cycling performance of sulfur cathodes with different binders with sulfur loading of 6.5 mg cm^{-2} at 0.8 mA cm^{-2}; (b) areal discharge capacity of the S@N-GG-XG electrode with sulfur loading of 6.5mg cm^{-2} at 0.8 mA cm^{-2}; (c) cycling performance and (d) coulombic efficiency of the S@N-GG-XG electrode with sulfur loading of 11.9 mg cm^{-2} at 1.6 mA cm^{-2}

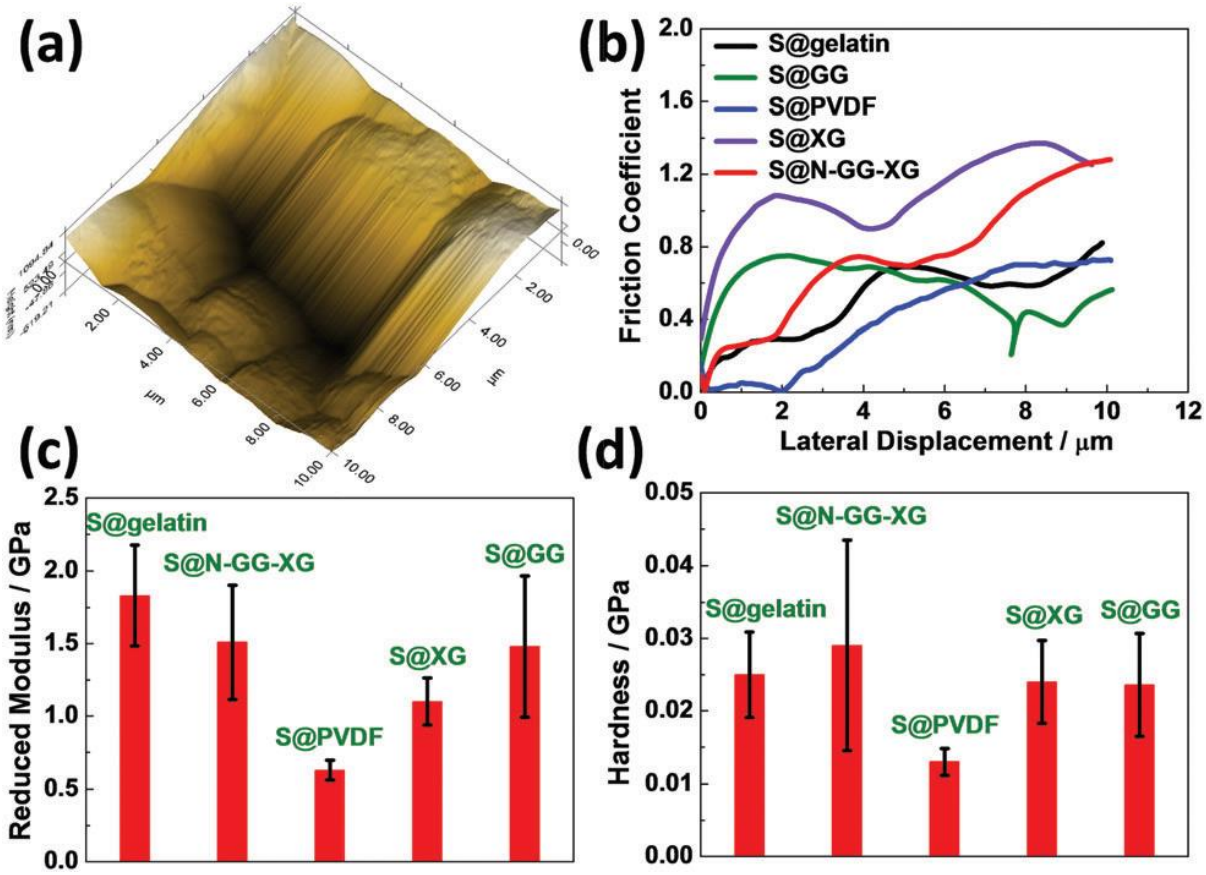

Fig. 4 Mechanical property evaluation: (a) in situ 3D nanoscratch image of the S@N-GG-XG electrode; (b) friction coefficients of sulfur electrodes with different binders obtained from the nanoscratch tests; (c) reduced modulus and (d) hardness of sulfur cathodes with different binders obtained from nanoindentation tests.

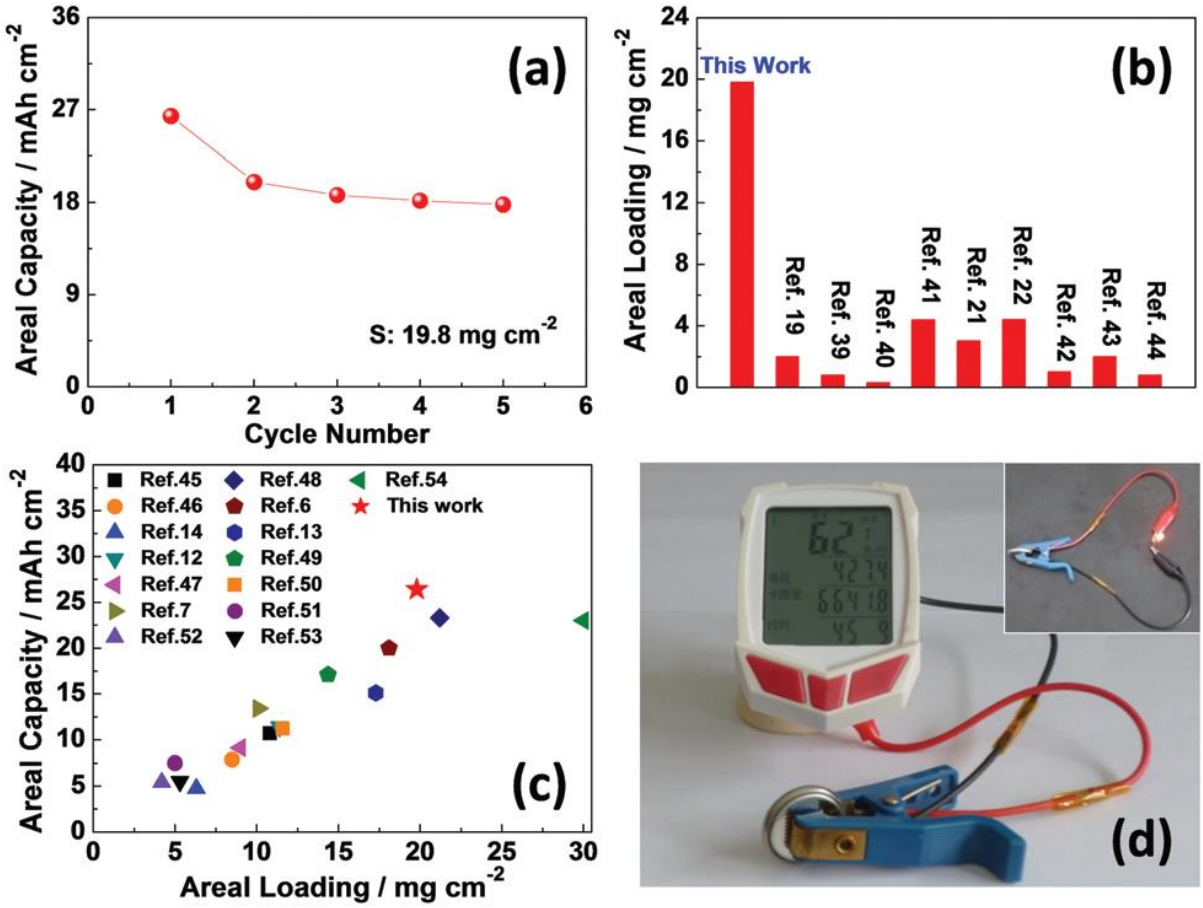

Fig. 5 (a) Cycling performance of the S@N-GG-XG electrode with sulphur loading of 19.8 mg cm^{-2}at 0.8 mA cm^{-2} (b) comparison of sulfur loading of Li–S batteries from some recent binder studies; (c) comparison of areal capacity and sulfur loading of Li–S batteries from some recent publications; (d) Li–S coin cell used to power an electronic stopwatch. Inset in (d) is a Li–S coin cell used to light a light-emitting diode.